DOI: https://doi.org/10.54966/jreen.v28i1.1339

Journal of Renewable Energies

Revue des Energies Renouvelables

journal home page: https://revue.cder.dz/index.php/rer

Conference paper

Photocatalytic properties of Mn_2O_3 nanoparticles synthesized via green chemistry method

Nadjah Sobti [a,*], Samiha Chaguetmi [b], Leila Amiour [c], Youcef Aouabdia [d], Lynda Saci [e]

[a] *Faculty of Natural and Life Sciences, University of Batna 2, Algeria*

[b] *Faculty of Sciences, University 20 August 1955 of Skikda, 21000 Skikda, Algeria*

[c] *Faculty of Exact Sciences, Constantine1 University, Constantine 25000, Algeria*

[d] *Ecole Normale Supérieur de Constantine Assia Djebar, Constantine 25000, Algeria*

[e] *LEMEAMED Laboratory, University of Constantine 1, 25000, Constantine, Algeria*

ARTICLE INFO

Article history:

Received January 21, 2025

Accepted January 29, 2025

Keywords:

Mn_2O_3,
Nanoparticles,
Green method,
Olive leaf extract,
Photocatalysis application.

ABSTRACT

The objective of this work is to synthesize Mn_2O_3 nanoparticles (NPs) using green method based on olive leaf extract (OLE). These nanoparticles are intended for photocatalytic applications, specifically the degradation of pollutants and dyes using methylene blue (MB) as a test substance. The synthesized material, initially described as manganese oxide (Mn_2O_3), was characterized using various techniques: thermogravimetric analysis (TGA), scanning electron microscopy (SEM), X-ray diffraction (XRD), FT-IR, Raman and UV-visible spectroscopies. Additionally, the photocatalytic tests were performed. XRD analysis revealed the formation of Bixbyite (Mn_2O_3) phases. Raman and FT-IR spectroscopy confirmed the presence of Mn-O bonds within the synthesized material. The TGA results supported the decomposition of organic compounds and the formation of the Mn_2O_3. The photocatalytic degradation tests with methylene blue yielded promising results. The addition of the synthesized material (Mn_2O_3) significantly enhanced the degradation of methylene blue, achieving an efficiency of 87.8%.

1. INTRODUCTION

Green chemistry goals is to reduce the risk reagents used in solid-state chemistry, encompassing the synthesis of nanoparticles (Zikalala et al., 2018; Clark, 1999; Duan et al., 2015). It substitutes organic solvents with solutions derived from water and replaces chemical components with natural extracts (Tuli et al., 2015). For instance, olive leaf aqueous extract (OLE) serves as a natural binder, while manganese acetate salt is employed as a source of metal ions. Olive leaf aqueous extract possesses antioxidant

* *Corresponding author, E-mail address: n.sobti@univ-batna2.dz*

ISSN: 1112-2242 / EISSN: 2716-8247

properties and can function as a chelating agent. This approach presents a cost-effective and sustainable alternative to traditional methods (Zikalala et al., 2018). The controlled synthesis of inorganic nanostructures, characterized by their size and shape, has been driven by the unique properties that depend on these dimensions, with the aim of realizing their practical applications (Gnanam et al., 2013; Vaseem et al., 2008). In recent years, there has been a significant focus on nanostructured manganese oxides due to their distinct electronic, magnetic, and catalytic properties (Banis et al.,2011; Ghosh et al., 2006; Lei et al., 2006), which differ markedly from those observed in their bulk counterparts, attributed to their anisotropic morphology, size, and shape (Nayak et al., 1999; Shanmugam et al., 2006). The most well-known inorganic manganese oxides, MnO, Mn_2O_3, and Mn_3O_4, find extensive applications in catalysis and battery technologies, highlighting their versatility and importance in these fields (Davar et al., 2009; Ahmad et al., 2004). Furthermore, the surfactant-assisted synthetic methods offer a convenient and powerful approach for the reproducible, controlled synthesis of nanocrystals. This is because these methods enable precise adjustment of the size, shape, composition, and phase structure of metal oxide nanocrystals at the nanometer scale (Zhang et al., 2005; Tang et al.,2002; Hou et al. 2005). In practically, Manganese (III) oxide (Mn_2O_3) represents an attractive transition metal oxide with a wide range of applications, including catalysis, energy storage, sensors, biomedical and environmental remediation (Thuille et al., 2003; Dey et al., 2020; Munir et al., 2024). Its remarkable stability, redox properties, and high surface area make it an ideal candidate for photocatalytic processes. Photocatalysis is the process that uses light energy to facilitate the acceleration of chemical reactions. Mn_2O_3 stands out among catalysts for the degradation of organic pollutants, such as methylene blue (MB), owing to its capacity to produce reactive oxygen species upon exposure to light. These reactive oxygen species subsequently oxidize the dye molecules, thereby decomposing them into more compounds that are benign. In this study, our objective was to synthesize manganese oxide nanoparticles (Mn_2O_3 NPs) employing a green chemistry approach. We focused on characterizing the resulting nanoparticles through various physical and chemical techniques, including X-ray Diffraction (XRD), Raman spectroscopy, Scanning Electron Microscopy (SEM), Fourier Transform Infrared Spectroscopy (FTIR), and thermogravimetric analysis (ATG). Additionally, we assessed the photocatalytic activity of these nanoparticles by measuring their ability to degrade an organic model substrate, methylene blue, dissolved in water, in the presence of Mn_2O_3 nanoparticles.

2. EXPERIMENTAL

OLE was obtained according to the following protocol. 5 g of fresh olive leaves were washed to remove impurities, dried, and then introduced in 100 ml of ultra-pure water. The mixture was then heated in a bottle of Rota Vap settled at 70° C for 3h. The color of the aqueous solution changes from watery to light yellow. Afterward, the extract solution was cooled down to room temperature and filtered in air (Sobti et al., 2021). Manganese oxide NPs were prepared then as follows. 20 ml of OLE yellow solution were added to 20 ml of a fresh aqueous manganese acetate (≥ 99.0%, from Sigma-Aldrich) solution (0.5 M). The mixture was introduced in a bottle of Rota Vap and heated at 70 °C for 3h. Then, the resulting solution was dried in a domestic microwave oven at 800 Hz for a period of 100 minutes, resulting in the formation of powder. The resultant product was washed with Milli-Q water and ethanol for five times and then dried at 60°C for 12h. This powder was then subjected to annealing at 500 °C for 1 hour to facilitate the crystallization of the desired Mn_2O_3 phase.

2.1 Characterization of Manganese Oxide NPs

Crystallographic structure of the produced powders was analyzed using a PANALYTICAL EMPYREAN X-ray diffractometer equipped with a Cu-K_α X-ray source. Raman spectroscopy was also

achieved on a HORIBA Lab RAM HR spectrophotometer equipped with a 473 nm laser source. Fourier Transform Infrared (FTIR) spectra were obtained using a SHIMADZU IRAffinity-1S Fourier Transform Infrared Spectrophotometer. The morphology of the samples was investigated by using a JEOL JSM-7100F scanning electron microscope (FEG-SEM) operating at 200 kV and Transmission electron microscopy (TEM) carried out on a JEM 2100 Plus microscope operating at 200 KV. The thermal decomposition behavior of powder was analyzed by thermogravimetric analysis (TGA Instruments, mark Mettler Toledo) from 25 to 500 °C at a scan rate of 10 °C/min in air atmosphere. Yield is a crucial quantitative characteristic for active materials.

2.2 Photocatalysis assays

The photocatalytic activity of the powder was assessed by measuring the degradation of a standard organic dye, methylene blue (MB), in an aqueous solution under ultraviolet (UV) light irradiation for various exposure times. The UV light source was a UV lamp (UV-VDL-15 UVB) with a power of 15 W, acquired from VILBER-Germany. Before starting the photocatalytic reaction, 20 mg of the powder catalyst, Mn_2O_3, was added to 100 mL of a methylene blue solution, which was already at a concentration of 15.6 10^{-6} mol/L. To ensure an adsorption-desorption equilibrium was reached before each irradiation, the solution was magnetically stirred in the dark for 30 minutes. The decomposition of methylene blue was evaluated using a UV-Vis spectrophotometer, with the maximum absorption wavelength of methylene blue being 660 nm (Chaguetmi et al., 2013). It represents the mass loss during pyrolysis. Commonly referred to as burn-off (Fernández-Ibáñez et al., 2003), the mass yield can be expressed using the following formula:

$$Yield = \frac{Final\ Mass}{Initial\ Mass} \times 100 \quad (1)$$

3. RESULTS AND DISCUSSION

The morphology of the produced Mn_2O_3 particles was analyzed using SEM and TEM microscopy.

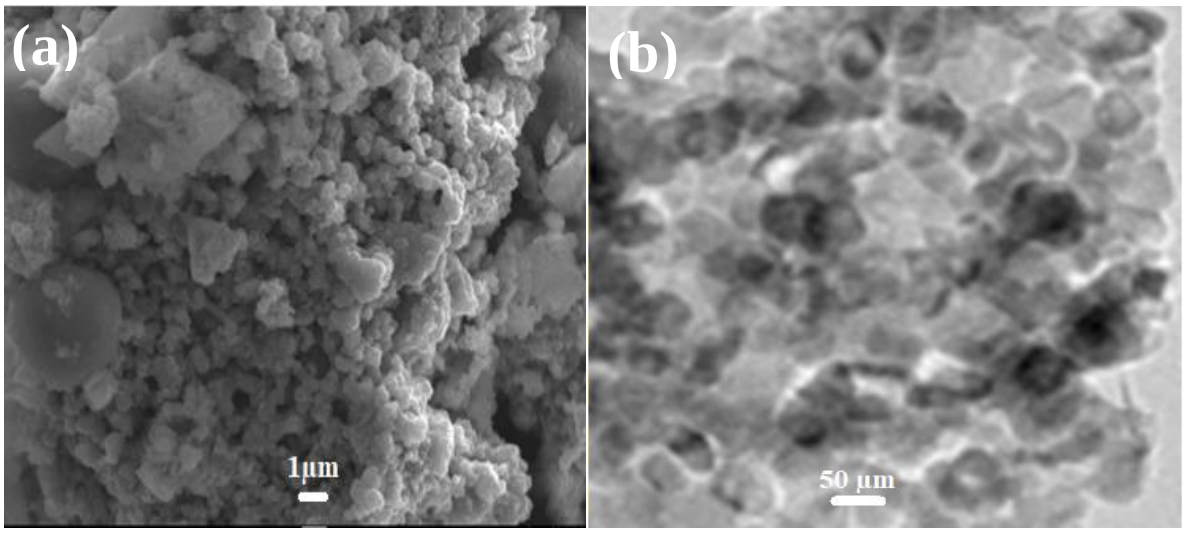

Fig 1. (a) SEM and (b) TEM images of Mn_2O_3 NPs**.**

Fig. 1(a) shows the distribution of manganese oxide nanoparticles and a number of aggregates, the particle shape was spherical. The mean size and distribution of nanoparticles were calculated using ImageJ software from FESEM micrographs. The approximate mean size of the nanoparticles was

determined to be between 23 and 80 nm in the FESEM image. Fig.1(b) shows the typical low-magnification TEM image of the Mn_2O_3. It confirmed the result obtained by the SEM analysis that the Mn_2O_3 exists in the spherical nanoparticles.

X-ray diffraction (XRD) analysis allows us to know the chemical composition of the products and the crystalline structure. The results are processed using High Score Plus software and PDF2 database.

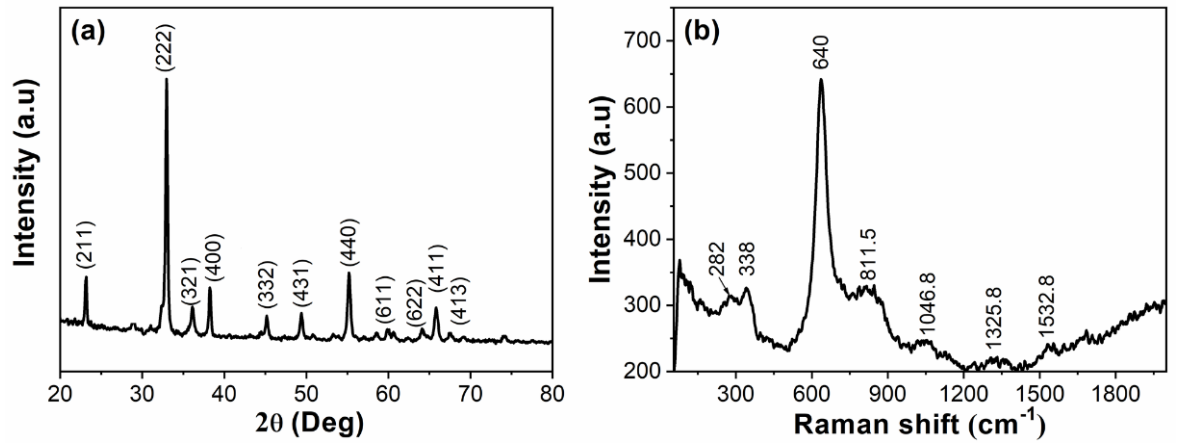

Fig 2. (a) XRD patterns and (b) Raman spectrum of Mn_2O_3 NPs

Fig. 2(a) shows the recorded XRD patterns on the annealed powder at 500°C. Interestingly, the pattern of the powder obtained after annealing appears to be cubic Bixbyite Mn_2O_3 phases (ICDD No. 98-007-6087). The peaks observed at 2θ: 23.2°, 32.9°, 36.1°, 38.2°, 45.2°, 49.3°, 55.2°, 59.9°, 64°, 65.9° and 68.9°, which can be attributed to the (211), (222), (321), (400), (332), (431), (440), (611), (622), 5411) and (413) plans for Mn_2O_3 NPs (Chandiran et al., 2020). There are no other diffraction peaks corresponding to impurities, indicating the high purity of the Mn_2O_3 NPs. This result is confirmed by Raman spectroscopy (Fig. 2(b)) since the spectrum collected on the powders annealed at 500 °C exhibits the exact signature of the cubic phases. The Raman spectrum of the powder exhibits both four bands centered at 282, 338, 640.5, and 811.5 cm^{-1}, which are usually attributed to the vibration mode of Mn-O-Mn in Mn_2O_3 (Gnanam et al., 2013; Han et al., 2006), as well a band at 640 cm^{-1}, characteristic of the Mn (III)-O vibration mode in Mn_2O_3 (Han et al., 2006; Davar et al., 2009; Gnanam et al., 2013). Another band appearing at 1046.8 cm^{-1} is due to the organic groups linked to Mn (Gnanam et al., 2013). Additionally, the Raman spectra of the sample display two broad peaks at 1325.8 and 1532.8 cm^{-1}. These peaks may be due to vibrations C−C, possibly from carbon contamination from a previous OLE adsorption process (Sobti et al., 2021).

Fig. 3(a) shows the FTIR spectrum of the resulting Mn_2O_3 nanoparticles. The weak bands observed around 2452 and 1638 cm^{-1} correspond to the stretching and bending vibration modes of O-H. Additionally, Mn_2O_3 exhibits two strong characteristic bands at 523 and 575 cm^{-1}, which are attributed to the stretching vibration modes of Mn-O (Davar et al., 2009; Gnanam et al., 2013). Moreover, the peak centered at 870 cm^{-1} may be related to the oxygen-containing functional groups of some additives present in OLE extrait. The peak at 1175 cm^{-1} is attributed to the C-OH stretching vibrations, while the band at 1531 cm^{-1} is due to C-O stretching (Sevilla et al., 2009; Zheng et al., 2010; Zheng et al., 2013). These findings suggest that organic residues, are present on the surface of the as-prepared Mn_2O_3 nanoparticles.

Thermogravimetric analysis (TGA) is used to measure changes in mass of a sample as a function of temperature and Differential Thermogravimetry (DTG) is the derivative of a TGA curve, which shows the rate of mass changes. Therefore, this method allows for the evaluation of thermal stability and the

determination of kinetic parameters during thermal decomposition, such as activation energy. Fig. 3(b) shows the comparison of TGA/DTG measurements recorded on powder during the heating of samples at 500°C under an oxygen flow. The first mass loss (1 mg, 9.90%) occurs in the temperature range between 30°C and 149°C, corresponding to the loss of water (release of residual water as vapor). The most significant loss, according to the derivative (DTG) curve, of 4.16 mg (41.37%), corresponds to the decomposition of the organic surfactant (OLE) at temperatures between 243°C and 340°C; the remaining mass (4.94 mg, 48.73%) corresponds to manganese trioxide (Mn_2O_3) (Gnanam et al., 2013). In addition, the yield calculation results for Mn_2O_3 under air conditions show a value of 48.9%.

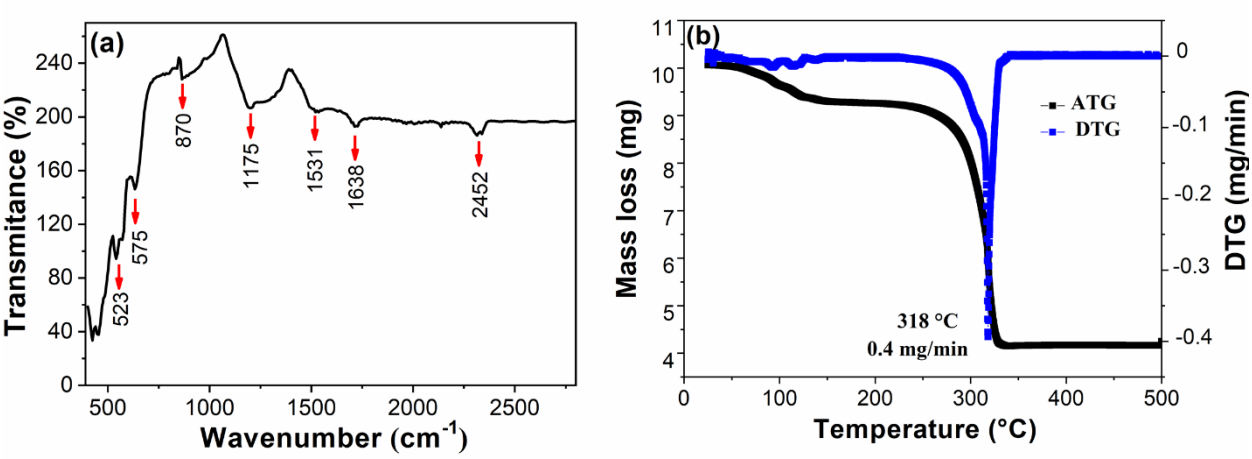

Fig 3. (a) FTIR spectrum of Mn_2O_3 NPs, (b) TGA and the derivative TDG curves recorded on the as-produced white powder at 500 °C.

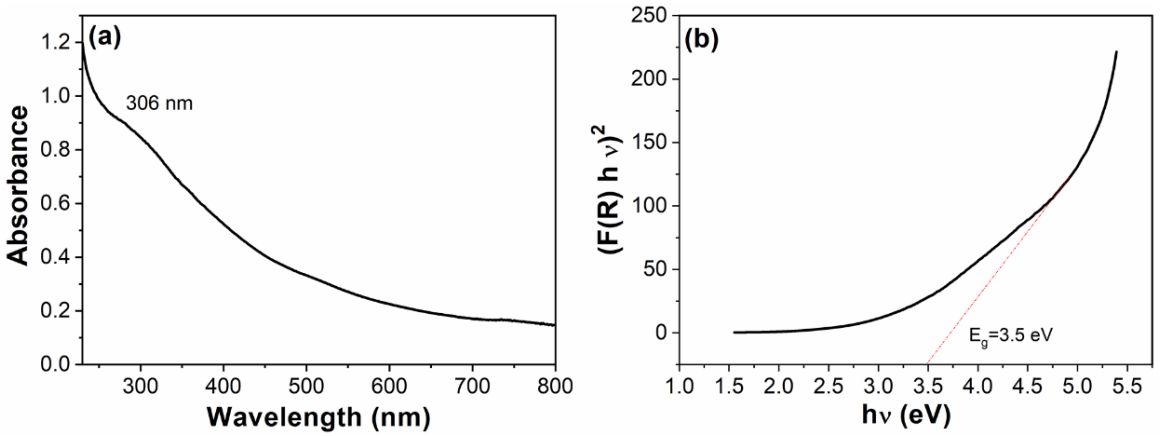

Fig 4. (a) Uv–vis absorption spectrum and (b) determination of the band gap of Mn_2O_3.

Fig. 4(a) shows an absorption peak at 306 nm of the Mn_2O_3 with an absorbance of 0.8%. The band gap energy calculated using the Kubelka–Munk method on the obtained powder of the Mn_2O_3, as depicted in Fig.4(b), is about 3.5 eV (Naeem et al., 2020).

The photocatalytic degradation of MB as a pollutant model by Mn_2O_3 NPs was evaluated by the absorbance of its characteristic band, centered at about 660 nm, in the optical spectra of a series of MB aqueous solutions irradiated by UV light for different times. Figure 5 gives these spectra for an exposure time of 1 h in the presence of Mn_2O_3 photocatalyst. The maximum intensity of the characteristic absorption peak of methylene blue at 660 nm decreased significantly after 20 min of irradiation compared to the absorption intensity at 10 min (as seen in Fig. 5). The decrease in the absorption peak

indicates that the double bond of the chromophore in the dye structure had been destroyed after irradiation with the Mn_2O_3 photocatalyst. The peak became progressively less intense with increasing irradiation time, signifying that sufficient photocatalytic reaction had occurred to destroy the dye chromophore (Davar et al.,2009; Gnanam et al., 2013).

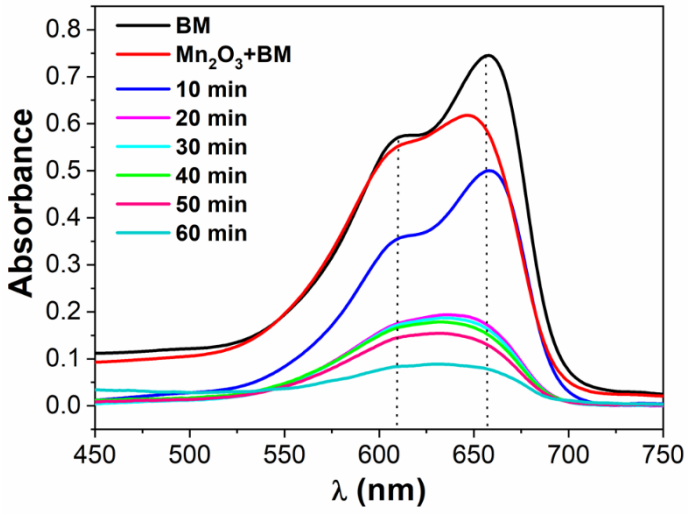

Fig 5. Photodegradation of MB in an aqueous medium using Mn_2O_3 NPs

Fig. 6(a) illustrates the plot of the relative concentration of MB (C(t)/C(t = 0)) as a function of radiation exposition time for the Mn_2O_3 catalyst. The photocatalytic capability of Mn_2O_3 nanoparticles was assessed through the degradation of MB solutions multiple times, thereby supporting the conclusion regarding the efficiency of Mn_2O_3 powder. The obtained results were found reproducible.

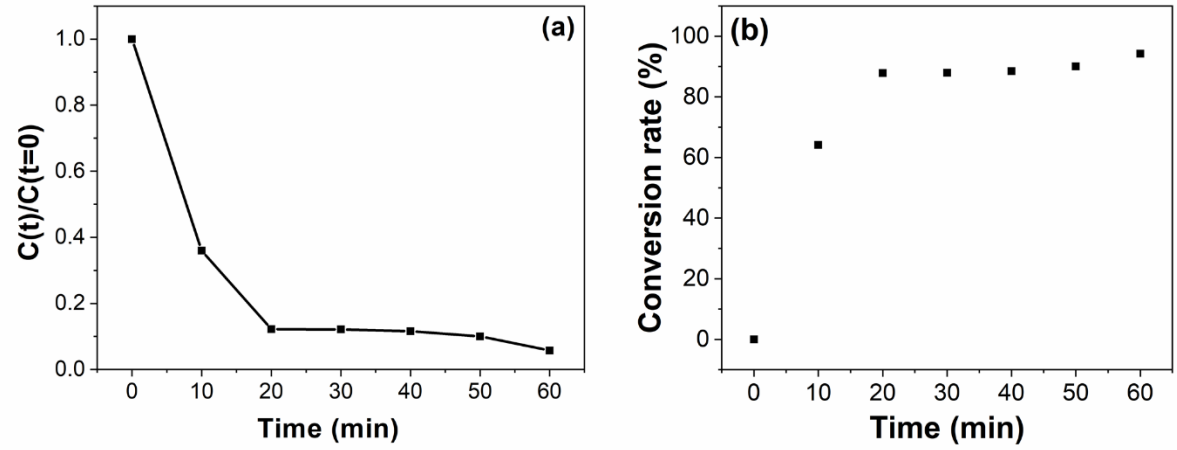

Fig 6. (a) Quantitative of the degradation of MB by Mn_2O_3 photocatalysts as a function of time, (b) Temporal evolution of the MB conversion during photodegradation by Mn_2O_3 NPs.

Using the provided data, the photodegradation conversion rate, $\boldsymbol{\tau}$, was calculated for the Mn_2O_3 catalyst:

$$\boldsymbol{\tau} = \frac{C_0 - C_t}{C_0} \times \mathbf{100} \qquad (2)$$

where C_0 represents the initial MB concentration (at t=0s) and C_t its concentration after a t irradiation time.

The variation of the calculated conversion rate as a function of UV exposure time was then plotted for the produced catalyst in Fig. 6(b). The final value after 60 minutes of irradiation time can give 87.8% as the photodegradation conversion rate.

For instance, a recent study that compared various synthesis methods found that the photodegradation efficiency of methylene blue was 85% for chemically synthesized Mn_2O_3 nanoparticles and 88% for those synthesized using green methods (used 100 mg of Mn_2O_3 catalyst for 120 min) (Amsaveni et al., 2020). Similarly, Gnanam and Rajendran explored the photocatalytic degradation of Remazol Red B using Mn_2O_3 nanodumbbells synthesized through hydrothermal methods with different ionic surfactants. They observed a maximum degradation efficiency of 71% (using 0.25 g of Mn_2O_3 catalyst for 4h) for the sample prepared with sodium dodecyl sulfate (Gnanam et al., 2013). Moreover, Chandiran et al. synthesized α-Mn_2O_3 nanorods through the hydrothermal method and assessed their effectiveness in decolorizing methylene blue and rhodamine B dyes. The degradation percentages of methylene blue (used 4.5 mg of Mn_2O_3 catalyst) at 120 minutes and rhodamine B at 70 minutes were recorded at 95% and 80%, respectively, underscoring the wide range of applications and potential efficiency of Mn_2O_3-based photocatalysts (Chandiran et al., 2020). Therefore, this study demonstrates superior degradation performance compared to previous research (Gnanam et al., 2013; Naeem et al., 2016; Chandiran et al., 2020).

4. CONCLUSION

The green chemical synthesis method was successfully employed to prepare manganese oxide nanoparticles. The SEM and TEM analysis revealed that the surface morphology of the powder consists of spherical nanoparticles, which are slightly agglomerated. Furthermore, XRD and Raman analysis show the cubic crystal structure of the Bixbyite Mn_2O_3. The TGA curves displayed a significant mass loss, signifying the decomposition of organic compounds in addition to the oxidation of Mn_2O_3. The photodegradation efficiency of methylene blue was found at about 87.8% by using the green chemical synthesized Mn_2O_3 nanoparticles as photocatalysts.

REFERENCES

Ahmad T, Ramanujachary KV, Loftland SV, Ganguli AK. (2004) Nanorods of manganese oxalate: a single source precursor to different manganese oxide nanoparticles (MnO, Mn_2O_3, Mn_3O_4). J. Mater. Chem, 14:3406-3410. https://doi.org/10.1039/B409010A

Amsaveni P, Nivetha A, Sakthivel C, Suresh Philip C, Prabha I. (2020) Effectiveness of surfactants for unique hierarchical Mn_2O_3 nanomaterials as enhanced oxidative catalysts, antibacterial agents, and photocatalysts. J. Phys. Chem. Solid, 144:109429. https://doi.org/10.1016/j.jpcs.2020.109429

Banis MN, Zhang Y, Banis HN, Li R, Sun X, Jiang X, Nikanpour D. (2011) Controlled synthesis and characterization of single crystalline MnO nanowires and Mn–Si oxide heterostructures by vapor phase deposition. Chem. Phys. Lett, 501: 470-474. https://doi.org/10.1016/j.cplett.2010.11.078

Chaguetmi S, Mammeri F, Nowak S, Decorse P, Lecoq H, Gaceur M, Ben Naceur J, Achour S, Chtourou R, Ammar S. (2013) Photocatalytic activity of TiO_2 nanofibers sensitized with ZnS quantum dots. RSC Adv, 3:2572-2580. https://doi.org/10.1039/C2RA21684A

Chandiran K, Murugesan RA, Balaji R, Andrews NG, Pitchaimuthu S, Nagamuthu Raja KC.2020 Long single crystalline α-Mn_2O_3 nanorods: facile synthesis and photocatalytic application. Mater. Res. Express, 7 (7):074001-074011. https://doi.org/10.1088/2053-1591/ab9fbd

Clark JH. (1999) Green chemistry: challenges and opportunities. Green. Chem, 1:1-8. https://doi.org/10.1039/A807961G

Davar F, Mohandes F, Salavati-Niasari M. (2009) Synthesis and characterization manganese oxide nanobundles from decomposition of manganese oxalate, Inorg. Chim. Acta, 362 :3663-3668.https://doi.org/10.1016/j.ica.2009.04.022

Dey S, Praveen Kumar VV. (2020) The performance of highly active manganese oxide catalysts for ambient conditions carbon monoxide oxidation, Current Res. Green and Sustainable Chem, 3: 100012-100027. https://doi.org/10.1016/j.crgsc.2020.100012

Duan H, Wan D, Li Y. (2015) Green chemistry for nanoparticle synthesis. Chem. Soc. Rev, 44: 5778-5792. https://doi.org/10.1039/C4CS00363B

Fernández-Ibáñez F, Blanco J, Malato S, de las Nieves FJ. (2003) Application of the colloidal stability of TiO_2 particles for recovery and reuse in solar photocatalysis. Water Research, 37: 3180-3188.DOI: 10.1016/s0043-1354(03)00157-x

Ghosh M, Biswas K, Sundaresan A, Rao CNR. (2006) MnO and NiO nanoparticles: synthesis and magnetic properties. J. Mater. Chem, 16:106-111. DOI: 10.1039/B511920K

Gnanam S, Rajendran V. (2013) Facile hydrothermal synthesis of alpha manganese sesquioxide (α-Mn_2O_3) nanodumb-bells: Structural, magnetic, optical and photocatalytic Properties. J. All. Compds, 550:463-470. https://doi.org/10.1016/j.jallcom.2012.10.172

Han YF, Chen FX, Zhong ZY, Ramesh K, Chen LW, Widjaja E. (2006) Controlled synthesis, characterization, and catalytic properties of Mn_2O_3 and Mn_3O_4 nanoparticles supported on mesoporous Silica SBA-15. J. Phys. Chem, 110:24450-24456.https://doi.org/10.1021/jp064941v

Hou Y, Kondoh H, Ohta T, Gao S. (2005) Size-controlled synthesis of nickel nanoparticles, Appl. Surf. Sci, 241:218-222. https://doi.org/10.1016/j.apsusc.2004.09.045

Lei S, Tang K, Fang Z, Liu Q, Zheng H. (2006) Preparation of a-Mn_2O_3 and MnO from thermal decomposition of $MnCO_3$ and control of morphology, Mater. Lett, 60: 53-56. https://doi.org/10.1016/j.matlet.2005.07.070

Munir G, Elsayed Ahmed Mohamed H, Hkiri K, Ghotekar S, Maaza M. (2024) Phyto-mediated fabrication of Mn_2O_3 nanoparticles using Hyphaene thebaica fruit extract as a promising photocatalyst for MB dye degradation. Inorganic Chemistry Communications, 167:112695-112703. https://doi.org/10.1016/j.inoche.2024.112695

Naeem R, Ali M, Rosiyah Yahya E. (2016) Fabrication of pristine Mn_2O_3 and Ag-Mn_2O_3 composite thin films by AACVD for photoelectrochemical water splitting. Dalton Transactions, 45:14928-14939. https://doi.org/10.1039/C6DT02656G

Nayak S K, Jena P. (1999) Equilibrium geometry, stability, and magnetic properties of small MnO clusters. J. Am. Chem. Soc, 121:644-652. https://doi.org/10.1021/ja981721p

Sevilla M, Fuertes AB. (2009) Chemical and structural properties of carbonaceous products obtained by hydrothermal carbonization of saccharides. Chem Eur J, 15: 4195-4203.DOI: 10.1002/chem.200802097

Shanmugam S, Gedanken A. (2006) MnO octahedral nanocrystals and MnO@C core-shell composites: synthesis, characterization, and electrocatalytic properties. J. Phys. Chem. B, 110: 24486-24491.https://doi.org/10.1021/jp0657585

Sobti N, Chaguetmi S, Achour S, Chaperman L, Mammeri F, Ammar-Merah S. (2021) Manganese oxide nanoparticles prepared by olive leaf extract-mediated wet chemistry and their supercapacitor properties. Journal of Solid-State Sciences, 113:106551-106558. https://doi.org/10.1016/j.solidstatesciences.2021.106551

Tang Z, Kotov NA, Giersig M. (2002) Spontaneous organization of single CdTe nanoparticles into luminescent nanowires. Science, 297:237-240. DOI: 10.1126/science.1072086

Thuille N, Fille M, Nagl M. (2003) Bactericidal activity of herbal extracts. Int. J. Hyg. Environ. Health, 206: 217-221. https://doi.org/10.1078/1438-4639-00217.

Tuli HS, Kashyap D, Bedi SK, Kumar G, Sandhu SS. (2015) Molecular aspects of metal oxide nanoparticle (MO-NPs) mediated pharmacological effects. Life Sci, 143:71-79.https://doi.org/10.1016/j.lfs.2015.10.021

Vaseem M, Umar A, Hahn YB, Kim DH, Lee KS, Jang JS, Lee JS. (2008) Flower shaped CuO nanostructures: structural, photocatalytic and XANES studies. Catal. Commun, 10:11-16.https://doi.org/10.1016/j.catcom.2008.07.022

Zhang Z, Sun H, Shao X, Li D, Yu H, Han M. (2005) Three-dimensionally oriented aggregation of a few hundred nanoparticles into monocrystalline architectures. Adv. Mater, 17:42-47. https://doi.org/10.1002/adma.200400401

Zheng M, Liu Y, Jiang K, Xiao Y, Yuan D. (2010) Alcohol-assisted hydrothermal carbonization to fabricate spheroidal carbons with a tunable shape and aspect ratio. Carbon, 48:1224-1233.https://doi.org/10.1016/j.carbon.2009.11.045

Zheng M, Zhang H, Gong X, Xu R, Xiao Y, Dong H, Liu X, Liu Y. (2013) A simple additive-free approach for the synthesis of uniform manganese monoxide nanorods with large specific surface area. Nanoscale Research Letters, 8:166-174. https://doi.org/10.1186/1556-276X-8-166

Zikalala N, Matshetshe K, Parani Oluwafemi SO. (2018) Biosynthesis protocols for colloidal metal oxide nanoparticles. Nano-Structures & Nano-Objects, 16:288-299. http://doi.org/10.1016/j.nanoso.2018.07.010.